Functional MR Imaging in intracranial and extracranial artery stenosis: evaluation of cerebral vasoreactivity with a breath-hold paradigm

PURPOSE

In the clinical practice cerebral vasoreactivity (CVR) can be evaluated by Trans-Cranial Doppler (TCD) examination or by Nuclear Medicine. In this study we test the feasibility of Functional Magnetic Resonance Imaging (f-MRI) to measure the CVR in patient with stenosis of internal carotid artery (ICA) or middle cerebral artery (MCA). The results were compared to those obtained by TCD.

MATERIAL AND METHODS

We enrolled 21 patients affected by stenosis of the internal carotid artery (ICA) or the middle cerebral artery (MCA). All patients underwent a 3 Tesla MR examination. Cerebral vasoreactivity was evaluated by a breath-hold f-MRI protocol. F-MRI data analysis was performed using FEAT tool of FSL package. Activation Maps in Regions of Interest (ROIs) of the MCA were obtained for each patient, with calculation of the percentage of activated voxels (% Act Vox) and the maximum (Z-max) and mean (Z-mean) values of the magnitude of the response. BOLD indexes (maximum peak, slope half-maximum, full-width half-maximum) were also obtained by placing ROIs in the cortex of temporal lobe, the occipital lobe, the temporal-occipital junction and in the central fissure.

The MR protocol also included MR-angiography and MR perfusion sequences.

A breath-hold TCD examination for the evaluation of cerebral vasoreactivity was performed in 12 of 21 patients.

A ROC curve analysis was performed to compare the accuracy of breath-hold FMR with respect to breath-hold TCD in detecting a reduced CVR.

RESULTS

CVR evaluated by breath-hold f-MRI was significantly reduced in the cerebral tissue irrorated by the stenotic vessels. The group of patients with occlusion/subocclusion had a BOLD-CVR significantly reduced with respect to the group with moderate stenoses. Perfusional data showed a moderate positive correlation between the CBF and the BOLD-CVR.

The ROC curve analysis demonstrated that breath-hold FMRI has an accuracy of 80% in detecting compromised CVR as identified by TCD.

CONCLUSIONS

fMRI with breath-hold paradigm is an alternative tool in the evaluation of cerebral vasoreactivity. Its advantages are the non-invasiveness, the operator-indipendence and the possibility to perform in the same examination also morphologic and angiographic sequences for a complete evaluation of brain parenchima and circulation. The measurement of BOLD response could also be helpful in the assessment of cerebral vasoreactivity in the subjects in which the trans-cranial Doppler examination is doubt, not diagnostic or not practicable.

INTRODUCTION

Definition of cerebral vasoreactivity

An adequate cerebral perfusion is necessary anytime to provide to the brain tissue the required amount of glucose and oxygen ($O_{2)}$ and to remove catabolites produced as carbonic dioxide ($CO_{2).}$ This physiological function is based on the vasomotricity which enables, through the dilation and contraction of the vessels, to adjust the cerebral blood flow in response to variations in neuronal activity (neurovascular coupling), cerebral perfusion pressure (autoregulation), circulating gases and metabolites (vasoreactivity).[1]

Neurovascular coupling refers to the variations of the cerebral blood flow in response to the neuronal activity. It is the result of the close interaction between neurons, glia and vascular cells, whereas the consumption of adenosine triphosphate (ATP), glucose and O_2 leads immediately to the release of vasoactive agents as potassium (K^+), nitric oxide (NO) and adenosine.[2,3] Autoregulation of blood flow is a regulatory mechanism that allows blood flow in a vascular bed to remain relatively constant during variations of arterial pressure. In the brain it is particularly developed and plays an important protective role against the risk of hypoxia at low perfusion pressure and of brain edema at higher arterial pressure.[4,5]

Cerebral Vasoreactivity, or Cerebrovascular Reactivity (CVR) refers to the capability of vasoconstriction and vasodilatation of the brain circulation in response to vasoactive substances (ions, neurotransmitters, circulating gases), with particular reference to O_2 and CO_2.[6] The main vasoactive substances and their effect on brain arterioles are summarized in table 1.

	DILATATION	CONSTRICTION
IONS	K^+	
	H^+	
METABOLITES	CO_2	O_2
	Adenosine	
NEUROTRANSMITTERS	Acetylcholine	Noradrenalin
	GABA	Serotonin
	Dopamine (D1/D5 receptors)	Dopamine (D2/D3/D4 receptors)
OTHERS	Nitric Oxide	

Table 1. Principal vasoactive substances. Adapted from Kramnik

In healthy subjects, CVR is influenced by sex, age, arterial pressure, basal perfusion conditions and modulation of vasomotor neuromodulators, such acetylcholine. In physiological conditions, the vasoreactivity is greater in the grey matter than in the white matter, and it is greater in the cerebral cortex than in the cerebellum.[7] Differences have also been reported within the cerebral cortex, with a more marked vasoreactivity in the occipital and frontal lobes.[8] In pathological conditions, CVR alterations have been observed in association with chronic arterial hypertension, diabetes, sepsis, antihypertensive drugs and opioid agonists administration. Variations of hemodynamic response have also been reported in the presence of diffused intracerebral factors such as microangiopathy, transient global amnesia, white matter diseases as CADASIL, normal pressure hydrocephalus, traumatic brain injury, Alzheimer's disease. Moreover, CVR impairment has been observed in consequence of locoregional alterations, such as arterial stenosis, focal epilepsy, stroke, arteriovenous malformations or tumors.[1]

Assessment of cerebral vasoreactivity

In occlusive cerebrovascular diseases, the cerebral vessels dilate to compensate for decreased cerebral perfusion pressure and to maintain Cerebral Blood Flow (CBF) in areas with compromised cerebral hemodynamics. Such areas are presumably vulnerable to ischemic brain injury after further reduction in perfusion pressure and are considered to have decreased cerebral perfusion reserve, best known as vascular reserve.[9,10] Assessing the CVR, the more clinically relevant and best measurable biomarker of vascular reserve, became crucial for the neurologist in order to identify the patient with increased risk of stroke or transient ischemic attack.[11,12] CVR assessments are commonly employed also in the pre- and postoperative evaluation of patients with occlusive cerebrovascular disease,[13,14] arteriovenous

malformations,[15] and chronic idiopathic hydrocephalus[16] and are possible intriguing tools in distinguishing vascular and Alzheimer's dementia.[17,18]

Several methods have been proposed to measure CVR, testing the response (vasodilatation, vasoconstriction, change of the oxygen extraction) to various stimuli (pCO^2 change, application of vasodilators, motor stimuli). Positron emission tomography (PET) with the assessment of oxygen extraction fraction (OEF) using the inhalation of ^{15}O-labeled gas is considered the "gold standard" of CVR examination.[19] Indeed, impairment in CVR, which lead to a reduction in CBF, can precede or occur alongside a compensatory increase in oxygen extraction state, sometimes referred to as "misery perfusion".[20] Other methods, which give indirect and semi-quantitative information about CVR, are computed tomography (CT) with administration of ^{133}Xe, perfusion CT, single photon emission computed tomography (SPECT) with ^{99m}Tc-HMPAO and near-infrared spectroscopy (NIRS).[21] However, PET examination is not widely available and the use of radiation makes most of these methodologies not suitable for longitudinal studies.[20]

For these reasons, non-invasive techniques have been developed. The most widely used hemodynamic imaging is the trans-cranial Doppler ultrasonography (TCD), a methodic that could be directly performed by the neurologist, associated with the clinical evaluation and easily repeatable. Assessment of CVR is performed by measuring the mean velocity (V_m) in basal conditions and after the induction of a vasomotor stimulus: a reduced acceleration of V_m after the induced vasodilatation reflects an impairment of CVR.[22,23]

More recently, advanced MR techniques have been proposed in non-invasive evaluation of cerebral vasoreactivity, such as Arterial Spin Labeling (ASL) perfusion methods and functional MR imaging with measure of BOLD response.[24,25]

Both techniques have advantages over TCD because they provide a better assessment of the regional distribution of vasoreactivity. The main advantage of fMRI techniques over of the ASL method is the better temporal resolution, although it is inferior than TCD but that allows a direct evaluation of the effect of the single vasomotor stimulus, in an analogue way to the assessment of neurovascular coupling (table 2).

Method	Measured variable	Advantages	Limitations
TCD	Ultrasound frequency shift reflecting flow velocity in large arteries	Temporal resolution (~1 sec); Indipendent of body position	Insonation window, angle and signal quality; Constant artery diameter assumption
3D-ASL MRI	Arterial H^+ spin tagging to measure blood flow	Spatial resolution; Non-invasive measurements of regional perfusion	Standard template; Signal averaging (~30s per whole brain); T1 time prolongation by hematocrit; Magnetic field inhomogeneities
BOLD-MRI	T2*-weighted imaging to detect differences in oxygenated and deoxygenated hemoglobin	Coupling between regional neuronal activity and blood flow, with a basis on changes of blood oxygenation	Indirect measure of blood flow and activity; Signal averaging (~5s); Standard template; Magnetic field inhomogeneities

Table 2. Advantages and limitations of the main non-invaisive methods for assessing CVR. Adapted from Novak

Concerning the vasodilatory stimulus, the most used drug is acetazolamide. ACZ inhibits carbonic anhydrase, which reversibly catalyses the conversion of CO_2+H_2O to H_2CO_3. It increases the H^+ and CO_2 concentration in the extracellular fluid of the brain, which is assumed to be the stimuli for the increasing in flow.[26] Alternatively, the inhalation of gas mixtures with variable higher concentration of CO^2 has been used.[27] However, the employment of intravenous drugs and the inhalation of gases make these investigations no longer non-invasive and more difficult to acquire. Although less accurate and dependent on the performance of the patient, the use of short period of apnea is always applicable and causes less patient discomfort.[21]

The better temporal resolution of TCD and BOLD f-MRI allows the use of breath-hold tasks and makes these examinations more easily achievable for a first evaluation of CVR. The better spatial resolution and the possibility to perform in the same examination a complete evaluation of brain parenchyma and vessels make f-MRI potentially superior to TCD. However, studies which employs f-MRI for the assessment of CVR are relatively few and with not standardized protocols.[28–31]

PURPOSE

The aim of this study is to investigate CVR in patients affected by intracranial or extracranial artery stenosis by using f-MRI with a breath-hold paradigm and to make a confrontation with TCD performed in the same patients.

MATERIAL AND METHODS

Patients

We enrolled 21 patients, 14 men and 7 women, with mean age of 63 years (range 27-80) followed by the Unit of Neurology of Azienda Ospedaliera Universitaria Pisana (AOUP) and previously diagnosed with stenosis of various grade of the Internal Carotid Artery (ICA) or of the Middle Cerebral Artery (MCA) by using ultrasonography, Computed Tomography (CT) Angiography or MR-angiography. 12 of 21 patients (57%) had a known history of symptomatic cerebrovascular accidents. All patients were Italians except one with African origin. The majority of subjects have past medical history of cardiovascular diseases, in particular hypertension (15/21, 71%). 52% of the patient were also affected by dyslipidemia (11/21), while only 3 patients were diabetics (14%). Smoking was a risk factor quite common in our population (11/21, 52%).

Demographic and clinical data of the patients are resumed in table 3.

N°	Sex	Age	Known vessel pathology	Hypertension	Diabetes	Dyslipidemia	Smoke	Other
1	M	57	Right MCA stenosis	Yes	No	Yes	No	African ethnicity
2	M	75	Bilat. MCA stenosis	Yes	Yes	No	No	Suspected vasculitis
3	F	54	Left ICA stenosis	Yes	Yes	Yes	No	
4	M	69	Bilateral MCA stenosis	Yes	No	No	Past	Suspected Moya-Moya
5	M	68	Right MCA stenosis	Yes	No	No	Past	
6	F	80	Left ICA stenosis	Yes	No	Yes	No	
7	F	72	Left MCA stenosis	No	No	Yes	No	Atrial Fibrillation
8	M	43	Right MCA stenosis	No	No	No	No	Suspected Moya-moya
9	M	75	Left ICA occlusion	Yes	No	Yes	No	
10	M	27	Right MCA stenosis	No	No	No	No	PFO, surg. Closed

N°	Sex	Age	Known vessel pathology	Hypertension	Diabetes	Dyslipidemia	Smoke	Other
11	M	64	Right MCA stenosis	No	No	No	Past	
12	M	75	Left ICA stenosis	Yes	No	Yes	No	
13	F	47	Left ICA stenosis	Yes	No	No	Yes	
14	F	54	Right ICA occlusion	Yes	No	Yes	Past	Job s.me; previous head injury
15	M	64	Left ICA stenosis	No	No	No	No	
16	M	67	Left ICA stenosis	Yes	No	Yes	Yes	
17	M	73	Right MCA stenosis	No	No	No	Past	Treated for Bladder ETP
18	F	71	Left ICA occlusion	Yes	No	Yes	Past	
19	M	60	Right MCA stenosis	Yes	Yes	Yes	Yes	LVH
20	M	71	Left ICA occlusion	Yes	No	No	Past	Iatrogenic occlusion
21	F	59	Left ICA occlusion	Yes	No	Yes	Yes	

Table 3. Demographic data, known vessels pathology and past clinical history of the enrolled patients. MCA: middle cerebral artery. ICA: internal carotid artery. PFO: patent foramen ovale. ETP: heteroplasia. LVH: left ventricular hypertrophy.

MR Protocol

All patients underwent to MR examination on 3 Tesla scanner (MR750, GE Healthcare, Milwaukee) with high performing gradients (gradients strength 80 mT/m, maximum slew rate 200 T/m/s), equipped with an 8-channel head coil with ASSET-technology.

The MR protocol included included TOF and Phase-Contrast (INHANCE) MR-angiography, Arterial Spin Labeling (ASL) perfusion Imaging and Echo-Planar fMRI sequence with a breath-hold paradigm. Conventional sequences included Three-Dimensional Fluid Attenuated Inversion Recovery (FLAIR-CUBE) and Diffusion Weighted Imaging (DWI) sequences.

According to the clinical question additional morphological sequences as Spin-Echo T1, Fast Spin-Echo T2 and Susceptibility Weighted Angiography (SWAN) has been performed. In some cases of carotid stenosis in which a more detailed imaging of the afferent vessel was requested, a Contrast Enhanced MR Angiography (CEMRA) after gadolinium injection has been added to the protocol.

Acquisition Data

The basic protocol lasted a total of about 30 minutes. A respiratory belt was fastened across each patient's chest to ensure that the patients followed the breathing instructions properly.

3-D FLAIR-CUBE was obtained with the following parameters: Scan Plane = Oblique; TR = 8000; TE = maximum; Slice Number = 126; Slice Thickness = 1,2 mm; Slab = 1,0; FOV = 26 cm; Phase-Fov = 1,00; NEX = 1; Matrix = 224x224; Bandwidth = 62,50; imaging time = 6:19 min.

DWI sequence was obtained with the following parameters: Scan Plane = Oblique; TR = 4400; TE = minimum; Slice Number = 32; Slice thickness = 4,00 mm; FOV = 22 cm; Phase-FOV = 1,00; Matrix = 160x224; Bandwidth = 250,00; asset acceleration factor = 2; b-value = 1000; diffusion direction = 3; frequency coding direction = R/L; phase coding direction = A/P; imaging time = 2:08min.

3D TOF protocol was used with the following parameters: TR = 23 ms, TE = 3,2 ms, flip angle = 20, slice thickness = 1 mm, overlap = 0,50 mm, matrix = 413x320, Bandwidht = 31,25, Field of View (FOV) = 20 cm, Phase-FOV = 0,80, voxel size = 0,4x0,5x1 mm, voxel volume = 0,2 mm^3, 5 slabs, RAMP pulse = I > S, MT pulse, flow compensation, EDR, ZIPx2, asset acceleration factor = 2; imaging time of 8:26 min. A presaturation band, concatenated with the acquisition slab, was applied above the imaging volume to saturate incoming venous blood.

3D INHANCE protocol was used with the following parameters: TR= minimum, TE = minimum, flip angle = 8, thickness = 1,2 mm, matrix = 384x256, Bandwidht = 31,25, FOV = 24 cm, Phase FOV = 1, voxel size = 0,6x0,9x1,2 mm, voxel volume = 0,65 mm^3, NEX = 1, VENC = 40; asset acceleration factor = 2; frequency coding direction = S/I; phase coding direction = A/P; imaging time of 6:14 min.

MR Perfusion consisted of a pCASL acquisition, with a delay equivalent to 1525 ms. pCASL acquisition has been obtained using gradient echo echoplanar images (EPI). Perfusional analysis with pCASL has been performed using the following parameters: Scan Plane = Axial, Freq FOV = 24, slice thickness = 4, freq. dir. = R/L, TR = 4632 ms, slab = 1, TE(s) per scan = 1, TE = 10,54 ms, flip angle = 111, Points = 512, Arms = 8, NEX = 3, Bandwidth = 62,5, Bo Maps = off, EDR, Fast, Spiral, auto, FOV = 24x31,7mm, post-labeling delay = 1525 ms; imaging time 4:29 min. Labeling was applied at the level of the cervico-medullary junction.

F-MRI data were obtained by a T2*-weighted gradient recalled multi-phase echo-planar imaging (EPI) sequence, sensitized to BOLD-effect and implemented with the following parameters: TR = 2500 msec; TE = 40 msec; Flip Angle = 90; matrix = 128×128; FOV = 26; Phase FOV = 0,90; NEX = 1; asset acceleration factor = 2; frequency coding direction = R/L;

phase coding direction = A/P; Multiphase with 100 phases for location. The sequence lasted 7:28 minutes.

f-MRI task

Before the breath-holding task, patients were required to breath naturally for at least five minutes. During fMRI scanning, patients were asked to hold their breath for 15 seconds and then to breathe naturally for the next 45 seconds. This cycle was repeated 7 times.

The checking of the respiratory triggering was the guarantee of a proper exercise. In the cases in which the exercise was not correctly observed the f-MRI sequence was performed again from the beginning.

Data analysis

F-MRI data analysis was performed using FEAT tool of FSL package (5.0 version), FMRIB's Software Library, Oxford University. Each functional data set underwent a pre-processing procedure including motion correction using MCFLIRT tool,[32] high pass temporal filtering (cut-off point = 100 s) and spatial smoothing (Gaussian kernel Full Width Half Maximum = 5 mm). In order to obtain spatially-resolved anatomical references for statistical maps, functional data sets were registered to brain-extracted 3D FLAIR-CUBE images by linear transformations with 6-degrees-of-freedom (FLIRT tool).[33,34] First-level statistical analysis was performed by GLM approach also including, in the design matrix, the head motion parameters estimated by MCFLIRT as adjunctive confound variables. BOLD activation maps were obtained using a physiological model instead of a block model using for each subject the values obtained in a reference ROI (12 mm^2) placed in the cortex of the temporal lobe of the healthy hemisphere (considering as healthy the hemisphere not affected by the vessel stenosis), in the territory of the MCA, and one placed in the cortex of the occipital lobe, in the territory of the PCA. Voxels with significant BOLD signal-intensity changes were determined with a corrected threshold of $z > 2.3$ ($p < 0.05$). The segmentation of the 3D images was obtained by using the Brainwave tool of a dedicated workstation (Advantage 4.5, GE Medical Systems). Then, functional and structural data sets were aligned to the Montreal Neurological Institute (MNI)-152 standard space (ICBM-152 template) to obtain comparable data forwithin and between group analyses. The number of statistically significant voxels was calculated in regions of interest of the left and right MCA territories and of the PCA territories (fig. 1A). In addition, we measured the maximum magnitude of the response (Z-max) and the mean magnitude (Z-mean) in the same ROIs calculated on the Activation Map without the application of a threshold.

ASL perfusion maps were analyzed by Functool software in the same workstation (Advantage 4.5, GE Medical Systems). Then, perfusion data sets were aligned to the MNI-152 standard space (ICBM-152 template) to obtain comparable data for within and between group analyses. The Cerebral Blood Flow data were calculated in the same ROIs of the left and right MCA territories and of the PCA territories.

In addition, smaller ROIs (volume 12 mm^2) were placed by a radiologist in the cortex of the temporal lobe, the occipital lobe, the temporal-occipital junction and in the central fissure by using the Multi-Image Analysis GUI (MANGO) software (3.4 version) (fig. 1B). For each ROI, we obtained the indexes of the ROI response, that are the maximum peak (MP), the slope half-maximum (SHM) and the full-width half-maximum (FWHM).

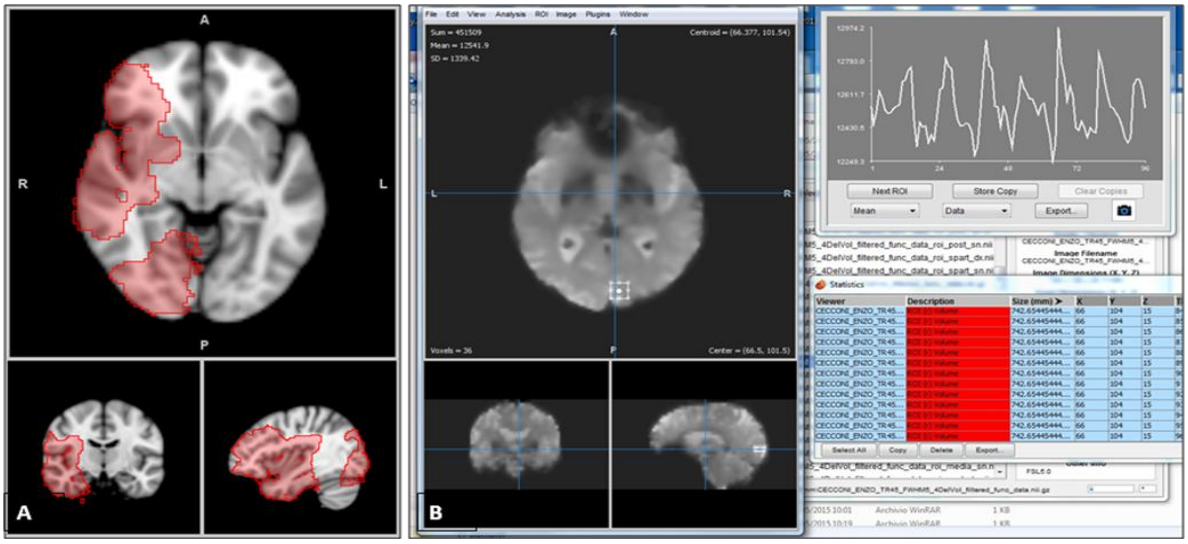

Figure 1. In A, the regions evidenced in red in the volumetric image represent the ROIs of the territory of the MCA and the posterior region in which % Act Vox, Z-max and Z-mean has been calculated. In B, filtered images elaborated with MANGO software with a small ROI placed in the cortex of the right occipital lobe (images are inversed with respect to the radiological convention). At top right, the relative BOLD curve shows the seven peaks corresponding to the seven periods of apnoea.

Doppler acquisition

Among the 21 patients of our study, 12 performed TCD (Embo-dop, Compumedics DWL, Germany) few days after MR examination. The exam was blindly conducted by an independent dedicated neurologist with a 2-MHz pulsed Doppler probe for insonation of cerebral vessels. After a standard TCD to locate the cerebral vessels, cerebral vasoreactivity was measured in both middle cerebral arteries via temporal windows, with the patient in a comfortable supine position. Hypercapnia was induced by a period of maximal apnea (at least 20 seconds). The cerebrovascular reserve was considered preserved if the percentage of the increase of the mean velocity of the MCA exceeded the 20%.[35,36]

RESULTS

MR data

All patients were able to complete the MR examination. Conventional sequences revealed in almost all subjects (20 of 21) vascular injuries of various degree, from small gliotic areas, mostly distributed in subcortical hemispherical white matter, corona radiata and basal ganglia, to large post-ischemic lesions corresponding to the areas of the previous and clinically known cerebrovascular accidents. In particular, the post-ischemic lesions involved the same hemisphere of vessels stenoses in 10 patients (48%). Among these, in two cases the gliotic scar involved part of the cortex included in the reference ROI of the activation map (fig. 2).

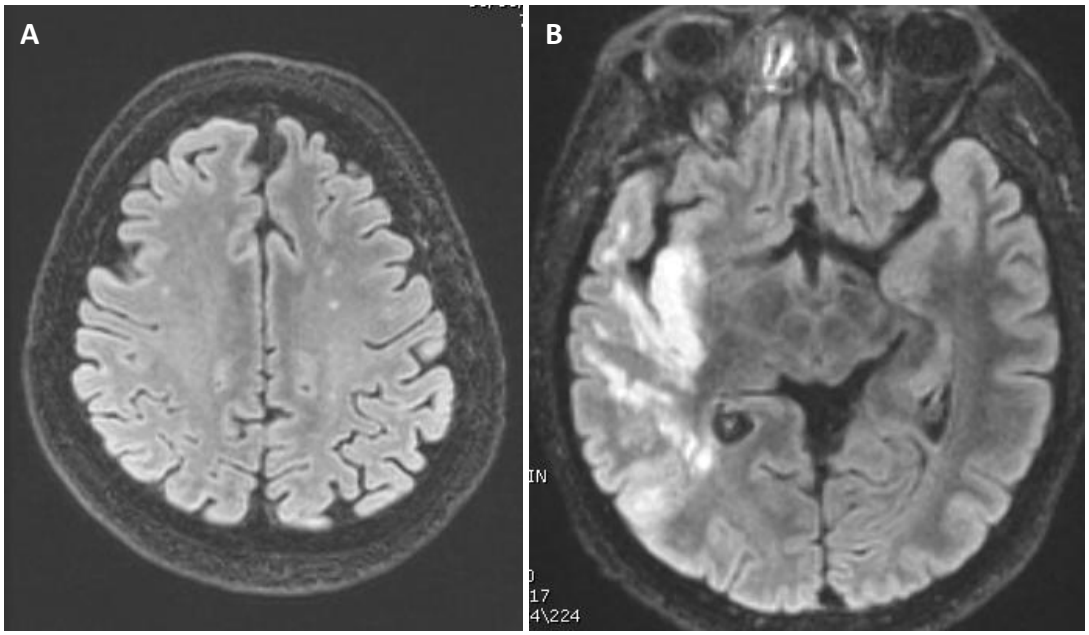

Figure 2. In A, FLAIR axial images of the pt 21 (female, 59 y.o.) shows only small gliotic areas in semioval centers, prevalent in the left side. In B, FLAIR axial images of the pt 19 (male, 60 y.o.) demonstrate a large post-ischemic lesion in the right temporal and insular lobes, regions included in the ROI used for the calculation of the BOLD response.

The only patient without brain significant findings was one of the younger (male, 43 years old). The only alterations with no vascular genesis revealed by conventional MR sequences were two small meningiomas in a male patient of 67 years and post-traumatic cortical-subcortical lesions in the anterior region of the frontal lobes in a female of 54 years.

MR-angiography sequences confirmed the presence of known intracranial MCA stenoses (fig. 3A). In extra-cranial stenoses, flow reduction or occlusion of the intracranial carotid artery with downstream reperfusion has been demonstrated (fig. 3B).

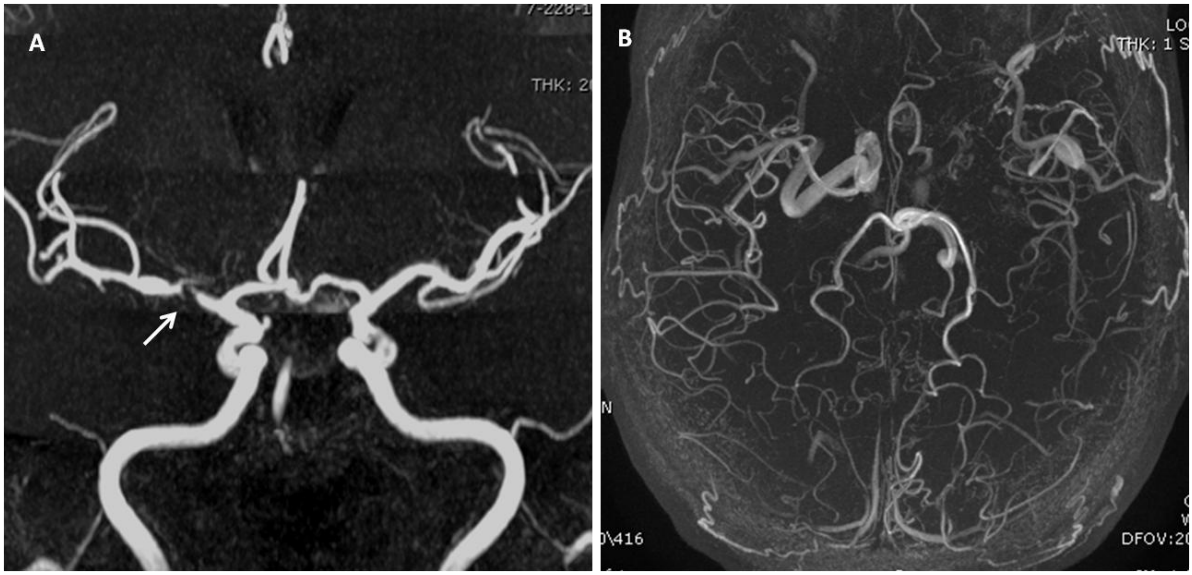

Figure 3. TOF-MRA angiography. In A, patient 11 (male, 64 y.o.): severe stenosis of the proximal tract of the MCA (arrow). In B, patient 9 (male, 75 y.o.). Intracranial MR-angiography demonstrated left internal carotid occlusion with flow reduction of the left MCA and the proximal tract of the ACA.

3D-INHANCE angiography allowed a better visualization of the upper tract of cerebral afferent vessels because of the more panoramic field of view and the higher contrast quality in proximal circle (fig. 3A).[37,38] When clinically requested, CEMRA was able to visualize the entire course of the neck vessels (fig. 3B).

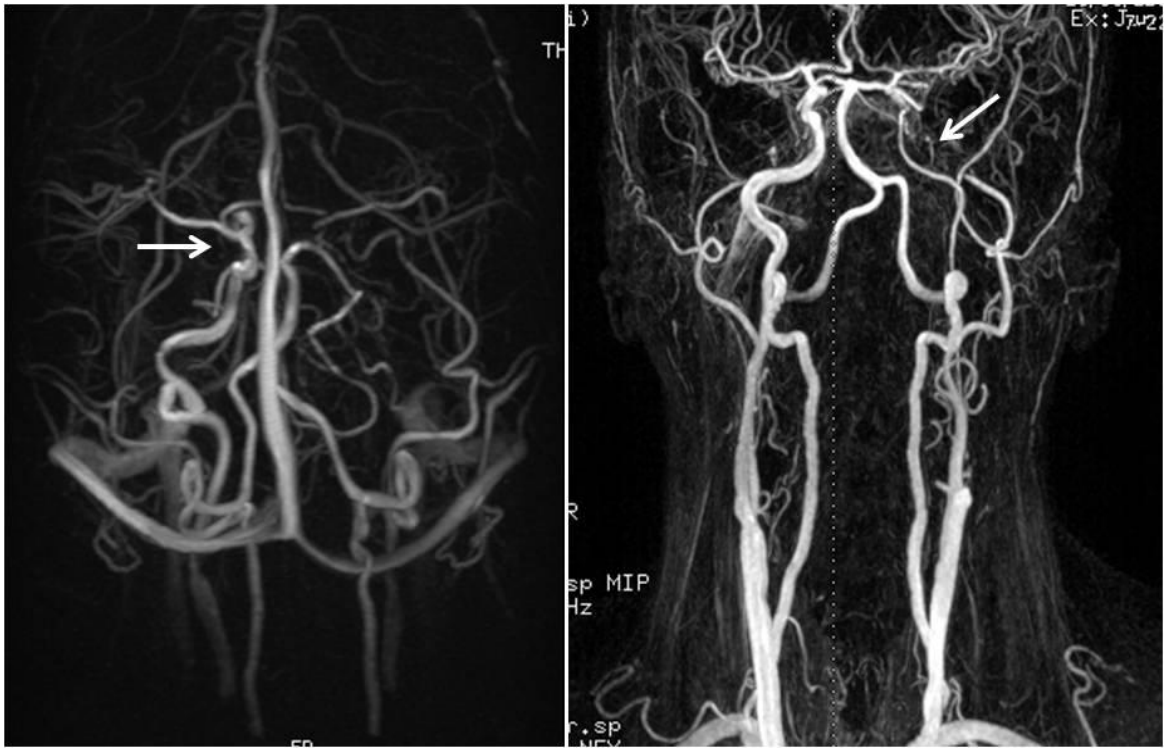

Figure 3. In A, 3D-INHANCE of patient 21 (female, 59 y.o.) with occlusion of the left ICA shows signal absence of the upper cervical and intra-cranial tracts of the artery. The right ICA is normally canalized (arrow). In B, CEMRA of patient 3 (female, 54 y.o.) affected by left ICA stenosis demonstrate threadlike impregnation of the carotid downstream to the bifurcation (arrow).

Two patients of 21 had bilateral MCA stenosis. In three patients we also observed stenoses of the Anterior Cerebral Artery (ACA). In one patient, stenoses of the Posterior Cerebral Arteries have been demonstrated. Furthermore, small aneurysms of the carotid siphon and of the MCA dichotomy have been discovered in two patients.

MR-angiography results and conventional sequences findings are reported in table 4.

N°	Sex	Age	MRA findings	Conventional MRI findings
1	M	57	mild reduction in calibre of right carotid siphon and proximal MCA	post-ischemic gliosis in right basal ganglia
2	M	75	stenosis, left distal ACA; reduction in calibre of MCA bilaterally;	mild bihemispheric leukoencephalopathy
3	F	54	left internal carotid stenosis	multiple post-ischemic lesions in left spartiacque territories
4	M	69	severe stenosis proximal MCA bilaterally (Moya-Moya like); stenosis left PCA; flow reduction in right PCA	gliotic scar prevalent in occipital lobes bilaterally
5	M	68	mild flow reduction in right distal MCA; left carotid siphon aneurysm (3 mm)	gliotic scar in right side of the pons; multiple areas of gliosis in basal ganglia, internal capsule and corona radiate
6	F	80	flow reduction left intracranial carotid artery	post-ischemic lesion of right internal capsule; periventricular leucoencephalopathy; frontal convolutions hemosiderosis
7	F	72	stenosis left proximal MCA	multiple areas of gliosis in basal ganglia, internal capsule and in parietal-temporal-occipital carrefour; lacunar infarcts in both cerebellar hemisphere
8	M	43	right MCA stenosis Moya-Moya like	no lesions
9	M	75	left internal carotid occlusion; flow reduction left MCA and ACA	post-ischemic scar right internal capsule; periventricular leucoencephalopathy
10	M	27	right carotid siphon stenosis; reduction in calibre of right ACM and ACA	post-ischemic scar in right basal ganglia, talamus, internal capusle and corona radiate
11	M	64	severe stenosis right proximal MCA	small gliotic areas in frontal lobes and pons
12	M	75	Unremarkable	periventricular and frontal-parietal subcortical leucopathy; multiple microhemorrages in basal ganglia, internal capsule and corona radiata
13	F	47	severe stenosis of left internal carotid artery; flow recovery in the siphon	small gliotic areas in semioval centers

N°	Sex	Age	MRA findings	Conventional MRI findings
14	F	54	left internal carotid occlusion; ACM dicotomy aneurysm (3mm)	post-traumatic scar cortical-subcortical frontal bilaterally and right temporal; post-ischemic scar right insula; subcortical bilateral frontal and left parietal gliosis
15	M	64	stent artifacts right IC; stenosis left IC; flow reduction left MCA	post-ischemic scar left frontal-parietal-occipital junction; gliosis right talamus, pons; periventricular leucopathy
16	M	67	Unremarkable	left clinoid and sphenoidal meningiomas; frontal bilateral and left peritrigonal gliosis
17	M	73	mild right distal MCA stenosis	left rolandic post-ischemic lesion
18	F	71	left IC occlusion; right proximal MCA stenosis	left frontal operculum and left temporal-parietal post-ischemic lesions
19	M	60	Severe stenosis of the inferior branch of MCA	post-ischemic lesion right of middle-upper temporal lobe, parietal-temporal-occipital temporal carrefour, posterior insula, basal rolandic sulcus
20	M	71	right internal carotid occlusion, mild flow reduction of right ACA and ACM	post-ischemic lesions of right parietal-occipital junction and left prerolandic and middle frontal lobe; gliotic areas left occiptal lobe, right rolandic sulcus, right middle frontal lobe, right cerebellar emisphere
21	F	59	Left ICA occlusion; left ACA stenosis; right MCA stenosis	Small gliotic areas in left semioval centers

Table 4. MR-angiography data and conventional sequences findings.

Doppler data

Among the 21 patients who performed MR examination, 12 were also investigated by TCD. CVR resulted preserved in 6 patients. In 4 patients, cerebrovascular reserve resulted compromised. In two of these subjects, the impairment was bilateral and symmetric.

In two patients, TCD was not diagnostic because of the high values of Vmean at basal evaluation with presence of aliasing artifacts.

Data of the TCD examinations are reported in table 5.

N°	Sex	Age	Vascular Reserve
1	M	57	Preserved CVR in right MCA territories; Vm increase = 36%
2	M	75	CVR compromised in both side; Vm increase = 15%
3	F	54	CVR seriously compromised in left side (Vm increase = 0%); CVR slightly compromised in right side (Vm increase = 17%)

N°	Sex	Age	Vascular Reserve
4	M	69	CVR compromised in both side (Vm increase = 14 %)
6	F	80	CVR preserved in both side (Vm increase = 35%)
7	F	72	CVR unobtainable because of aliasing artifacts
9	M	75	Preserved CVR in right side (Vm increase = 30%); CVR compromised in left side (Vm increase = 11%)
11	M	64	CVR unobtainable because of aliasing artifacts
13	F	47	CVR preserved in both side (Vm increase = 29%)
15	M	64	CVr preserved in both side (right Vm increase = 35%, left Vm increase = 25%)
16	M	67	CVR preserved in both side (Vm increase = 38%)
17	M	73	CVR preserved in both side (Vm increase = 30%)

Table 5. TCD data.

Healthy hemisphere parameters

The healthy hemisphere of each subject was studied by analysing the BOLD indexes of the ROIs placed in the cortex of the temporal lobes and the activation maps parameters obtained by using as models of response a ROI placed in the cortex of the temporal lobe of the healthy temporal hemisphere and a ROI placed in the cortex of the occipital lobe. We considered as healthy the hemispheres not affected by intra-cranial or extra-cranial stenoses. For this reason, in this analysis we discarded the two patients (n° 2 and 4) in which the stenosis was bilateral.

BOLD indexes are reported in table 6. We considered the mean of the maximum peak (MP) and the slope half-maximum (SHM) and the MP, the SHM and the full-width half-maximum (FWHM) of the highest curve of the exercise. The mean of the FWHM was not considered because of the high dispersion of the sample.

N°	Sex	Age	MP mean	MP max	SHM mean	SHM	FWHM
1	M	57	1.296	1.939	0.145	0.26	9.619
3	F	54	2.163	2.629	0.322	0.477	9.06
5	M	68	1.981	3.061	0.23	0.11	24.172
6	F	80	5.754	11.171	0.779	1.901	13.354
7	F	72	1.95	2.665	0.223	0.147	14.888
8	M	43	2.119	2.807	0.251	0.099	15.398
9	M	75	2.496	2.839	0.269	0.345	17.469
10	M	27	1.778	2.102	0.178	0.08	19.78
11	M	64	3.602	4.515	0.476	0.323	12.683
12	M	75	3.735	4.469	0.336	0.357	14.249
13	F	47	2.421	2.772	0.342	0.36	12.907

N°	Sex	Age	MP mean	MP max	SHM mean	SHM	FWHM
14	F	54	3.06	3.738	0.411	0.535	14.5
15	M	64	1.416	1.72	0.21	0.186	23.167
16	M	67	2.419	3.078	0.218	0.185	26.462
17	M	73	2.563	4.698	0.4	0.973	18.415
18	F	71	3.519	4.396	0.543	0.789	40.597
19	M	60	3.378	5.057	0.593	0.538	16.015
20	M	71	6.323	7.583	0.893	1.024	18.834
21	F	59	3.163	4.347	0.274	0.572	10.135

Table 6. BOLD indexes of MCA territory ROIs in the healthy hemisphere of the considered 19 patients. FWHM values are expressed in seconds.

Analyzing the indexes for all the subjects, we obtained for the MP mean a mean of 2.90, a median of 2.50 and a standard deviation (SD) of 1.32, with a confidence interval (CI) of ±0.59 (significance level 0.05). For MP maximum we obtained a mean of 3.98, a median of 3.08 and a SD of 2.23, with a confidence interval (CI) of ±1.00. For the SHM mean we obtained a mean of 0.37, a median of 0.32 and a SD of 0.20, with a confidence interval (CI) of ±0.09. For the SHM maximum we obtained a mean of 0.49, a median of 0.36 and a SD of 0.44, with a confidence interval (CI) of ±0.20. For the FWHM maximum we obtained a mean of 17.46", a median of 15.40" and a SD of 7.38", with a confidence interval (CI) of ±3.32.

Activation map parameters are reported in table 7. We considered, in the ROI of the MCA territory of the healthy hemisphere, the percentage of the activated voxels (% Act Vox) with a cluster threshold of 2.3 (p 0.05), the Z maximum and the Z mean without the application of a threshold. The values obtained by using a ROI in the MCA territory and a ROI using a ROI in the PCA territory are both reported.

			Activ Map with MCA ROI reference			Activ Map with PCA ROI reference		
N°	Sex	Age	% Act Vox	Z Max	Z mean	% Act Vox	Z Max	Z mean
1	M	57	81.7	16.1	5.5	83.1	11.8	5.2
3	F	54	69	13.1	4.1	53.7	6.5	2.7
5	M	68	46.1	11.3	2.7	53.8	7.5	2.6
6	F	80	53.1	12.6	2.8	17.6	6.7	1.5
7	F	72	33.9	10.4	2.4	39.8	9.1	2.4
8	M	43	76.6	13.9	4.7	73.2	10.5	4.1
9	M	75	48.9	11.7	2.8	26.6	6.6	1.7
10	M	27	72.2	15.7	5.7	75.5	11.7	5.5
11	M	64	74.4	13.2	4.6	69.6	8.3	3.6
12	M	75	75.8	13	5.2	78.2	11.4	4.7
13	F	47	51.6	16.1	3.6	42	7.5	2.3
14	F	54	75.4	16.9	4.3	70	10.2	3.9
15	M	64	53.7	12.2	3.2	22.2	5.5	1.6
16	M	67	58.1	13.6	3.8	62	9.9	3.6
17	M	73	64.5	14	3.8	57	9.8	3.2
18	F	71	54.7	11	3.1	59.4	8.4	3.2

			Activ Map with MCA ROI reference			Activ Map with PCA ROI reference		
N°	**Sex**	**Age**	**% Act Vox**	**Z Max**	**Z mean**	**% Act Vox**	**Z Max**	**Z mean**
19	M	60	63.8	16.7	3.3	57.2	8.5	2.9
20	M	71	73.4	10.3	3.8	70.3	9.6	3.7
21	F	59	65.7	13.2	3.9	60.3	8.7	3.2

Table 7. Activation maps parameters of the MCA ROIs of the healthy hemisphere, considering as models of response ROIs placed in the temporal lobe of the healthy temporal hemisphere and in the occipital lobe.

Analyzing the indexes for all the subjects for the activated maps modeled on the ROIs placed in the MCA territory, we obtained for the % Act Vox a mean of 62.77%, a median of 64.50% and a standard deviation (SD) of 12.82%, with a confidence interval (CI) of ±5.76. For the Z maximum we obtained a mean of 13.42, a median of 13.20 and a SD of 2.08, with a confidence interval (CI) of ±0.93. For the Z mean we obtained a mean of 3.86, a median of 3.80 and a SD of 0.96, with a confidence interval (CI) of ±0.43.

Considering the indexes of the activated maps modeled on the ROIs placed in the PCA territory, we obtained for the % Act Vox a mean of 56.39%, a median of 59.40% and a standard deviation (SD) of 19.01%, with a confidence interval (CI) of ±8.55. For the Z maximum we obtained a mean of 8.85, a median of 8.70 and a SD of 1.84, with a confidence interval (CI) of ±0.83. For the Z mean we obtained a mean of 3.24, a median of 3.20 and a SD of 1.14, with a confidence interval (CI) of ±0.51.

Correlation with age

Correlation coefficient (*r*) was calculated among the age of our population and every index of the BOLD response curve and Activation Map. A moderate negative correlation was found between the age and Z-max and Z-mean, particularly for the Activation Maps obtained from the MCA ROIs (respectively, r = -0.62 with p-value = 0.005 and r = -0.59, with p = 0.007), while for the PCA modeled indexes only Z mean was noteworthy (r = -0.50, with p = 0.03). A weakly positive correlation was conversely found between age and Maximum Peak of the highest curve of the BOLD response, with r = 0.50 (fig. 4).

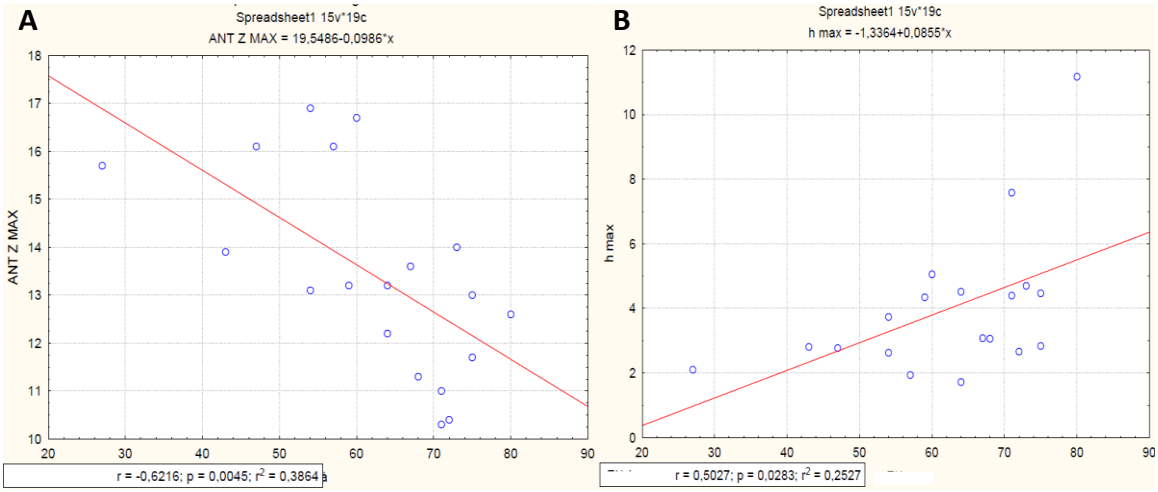

Figure 4. Correlation with age. In A, the scatter plot demonstrate a moderate negative correlation between age Zmax (r = 0,62). In B, the scatter plot shows a lower ma noteworthy positive correlation between age and maximum peak (r = 0.50).

Influence of comorbidities

Although statistically not significant ($p > 0.05$), a certain influence of the principal risk-factors over the Z-mean has been found despite the low number of patients. In particular, lower values of Z-mean have been found in the groups of patients with hypertension, dysplipidemia and in the smokers. The exiguous number of diabetic subjects (only 3) does not allow a more confident evaluation (fig. 5).

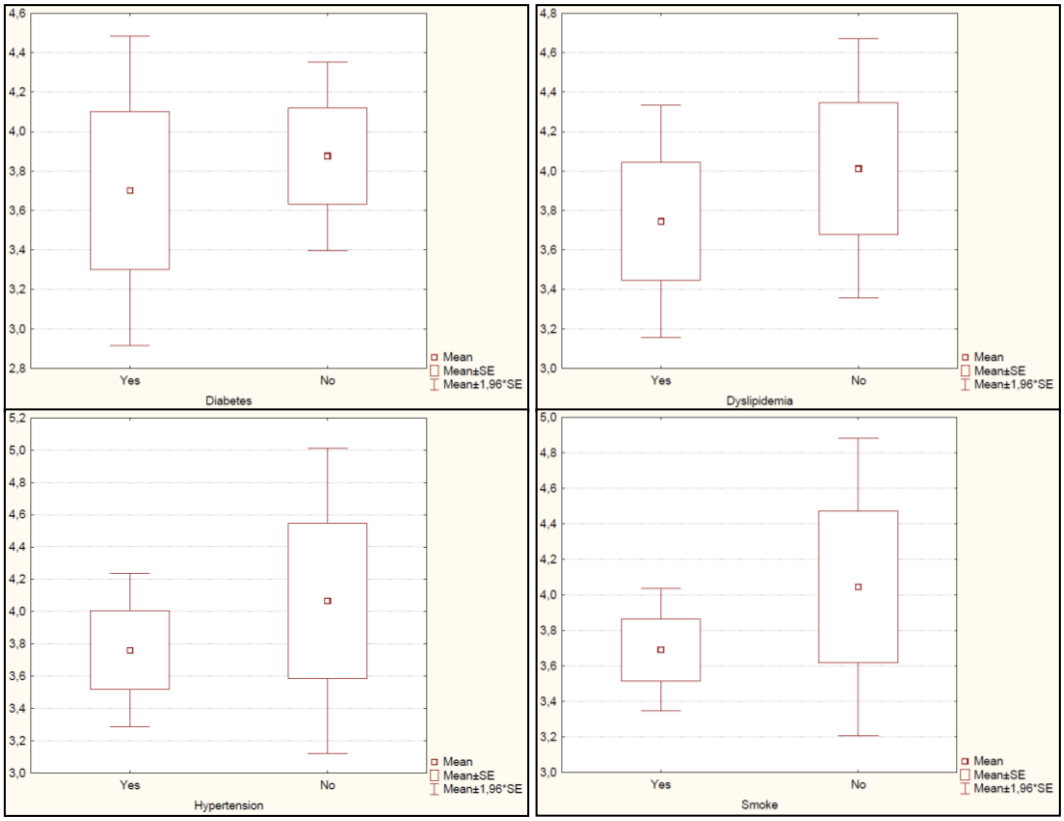

Figure 5. Box-plots in which the groups of patients with and without the main cardiovascular risk factors are matched for the Z-mean. The factors that seem more related to lower values of Z-mean are dyslipidemia and smoke.

Posterior circulation data

Data obtained from the Activation Maps in the ROIs covering the occipital lobes, in the vascular territory of the PCA, are resumed in table 7. As expected, the values are higher in the maps gained using a posterior small ROI as reference. However, as for the anterior circulation data, the negative correlation with age is more significant using the MCA ROI BOLD response as model, and specifically for the parameters Z-max e Z-mean, with values of *r* respectively of -0.62 and 0.63.

	Reference ROI in MCA			**Reference ROI in PCA**		
	% Act Vox	**Z Max**	**Z mean**	**% Act Vox**	**Z Max**	**Z mean**
Mean	69.17	9.06	3.95	73.03	10.94	4.38
Median	67.60	9.00	3.70	79.50	11.00	4.40
Std. Dv.	14.75	1.31	1.17	17.64	2.03	1.48
Conf. int.	6.63	0.59	0.53	7.93	0.91	0.66
Corr. with age	-0.47	-0.62	-0.63	-0.44	-0.24	-0.49

Table 7. Activation maps parameters of the PCA ROIs covering the occipital lobes, considering as models of response ROIs placed in the temporal lobe of the healthy temporal hemisphere and in the occipital lobe.

Healthy versus affected hemispheres confrontation

The data of the activation maps obtained before for the MCA vascular territory of the healthy hemispheres has been matched with the values obtained from the same analyses in the hemisphere affected by the intra-cranial or extra-cranial stenosis. Two statistical tests has been used for the confrontation, the *t-test for dependent samples* and the *Wilcoxon Matched Pairs Test*.[39,40] The results are resumed in the tables 8 and 9. Also for these analyses the number of subjects (*n*) was reduced to 19, considering both the hemisphere of the patients affected by bilateral MCA stenosis as affected and consequently not eligible for the confrontation.

Variable	**Mean**	**Std. Dv.**	**t-test for dependent samples p-value**	**Wilcoxon Matched Pairs Test**
ANT H % Act Vox	62.76842	12.82091	0.000306	0.000398
ANT A % Act Vox	47.89474	19.16262		
ANT H Z-max	13.42105	2.078081	0.000002	0.000182
ANT A Z-mean	9.45263	2.079094		

Variable	Mean	Std. Dv.	t-test for dependent samples p-value	Wilcoxon Matched Pairs Test
ANT H Z-mean	3.857895	0.957610	0.000034	0.000197
ANT A Z-mean	2.989474	1.098431		
POST H % ActVox	56.39474	19.00913	0.004146	0.003763
POST A % ActVox	45.10000	22.7135		
POST H Z-max	8.852632	1.844321	0.036644	0.038222
POST A Z-max	8.289474	2.244721		
POST H Z-mean	3.242105	1.135936	0.001488	0.002139
POST A Z-mean	2.768421	1.263176		

Table 8. T-test for dependent samples and Wilcoxon Matched Pairs Test for the confrontation of the MCA territory between healthy and affected hemisphere, considering as models of response ROIs placed in the temporal lobe (ANT) of the healthy temporal hemisphere and in the occipital lobe (POST). H = healthy hemisphere, A = affected hemisphere.

Using both the test, values in the MCA territories of the affected hemisphere are significantly lower with respect to the hemisphere without vessel stenosis. The value of *p* is lower of 0.01 considering all the parameters in the data obtained using a MCA ROI curve as reference. However, this result could be magnified by the fact that the reference ROI is placed in the healthy hemisphere. In particular the Z-max should be not taken in account, because in the healthy hemisphere it coincides with the reference ROI.

Using a posterior ROI as reference, the value of *p* increases but it still remains under the value of 0.01 for all the indexes except for the Z-max (0.04). Definitely, the value of Z-mean seems to be the more sensitive in distinguishing affected and not affected hemisphere, but also the percentage of activated voxels is reliable indicator.

Intra-cranial versus extra-cranial stenoses

In order to understand how the localization of the stenoses could influenced the indexes of BOLD response we divided the patients in two groups, one with the affected by internal carotid stenosis and the other with the affected by middle cerebral artery stenosis and we made a confrontation between the two groups using the Activation Maps parameters of the affected hemisphere obtained by using the MCA ROI of the healthy hemisphere as reference.

We also added another parameters, the lateralization index of the Z-mean, which best express the difference of activity between the two hemisphere. The lateralization index (LI) was calculated by the formula

$$\mathrm{LI} = \frac{A_\mathrm{L} - A_\mathrm{R}}{A_\mathrm{L} + A_\mathrm{R}},$$

where AL and AR refer to values of fMRI-measured activity for equal ROIs within the left (L) and right (R) hemisphere. A positive value of LI represents left-hemisphere dominance, a

negative value right-hemisphere dominance. The intermediate values reflect varying degrees of laterality.[41,42] In our analyses we used the absolute values of LI, considering the healthy hemisphere as dominant independently from the side. In the confrontation of the LI index we did not included the two patients with bilateral MCA stenosis.

The group with MCA stenosis consisted in 10 patients (mean age 60.80), with in the affected hemisphere a % Act Vox mean of 52.49% with St. Dv. 16.83, Z-max mean 10.00 with St. Dv. 1.96, Z-mean mean of 3.24 with St. Dv. 1.10 and LI mean of 0.11 with St. Dv. 0.10.

The group with ICA stenosis consisted in 11 patients (mean age 61.76), with, in the affected hemisphere, a % Act Vox mean of 43.99% with St. Dv. 19.23, Z-max mean 9.10 with St. Dv. 1.24, Z-mean mean of 2.72 with St. Dv. 0.58 and LI mean of 0.17 with St. Dv. 0.08.

The t-test demonstrated not statistically significative differences between the two groups ($p > 0.05$), although the patients with carotid stenosis showed higher dispersivity of the values between healthy and affected hemisphere with subsequent higher values of LI and mean lower values of the indexes of the Activation Map (fig. X).

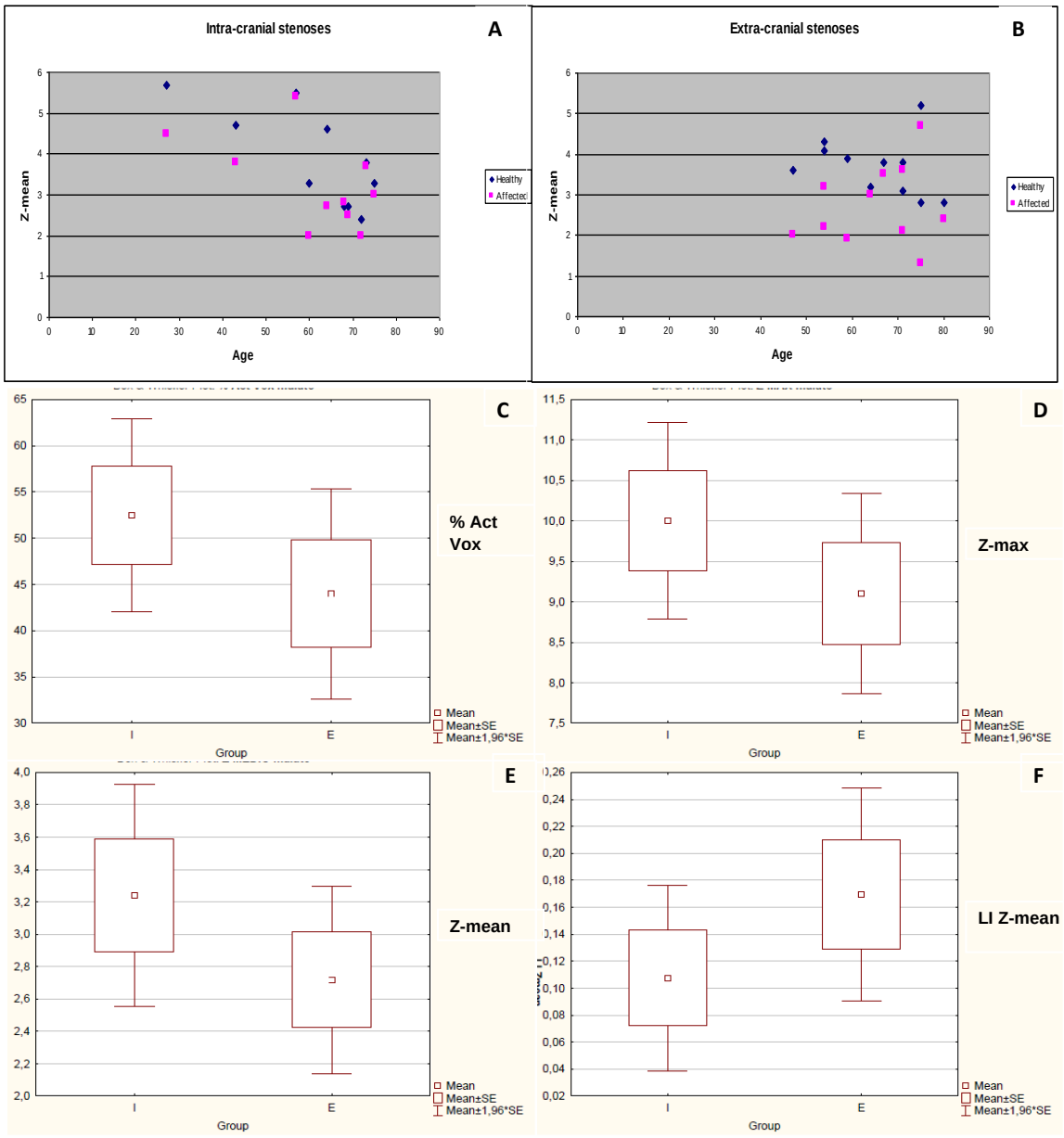

Figure 6. Confrontation between intra and extra-cranial stenoses. In A and B, scatter plots of the Z-mean in intra-cranial and extra-cranial groups, respectively, shows higher dispersivity between healthy and affected hemisphere in the extra-cranial group. In C-E, box plots shows lower values of the Activation Map parameters in the patients with carotid stenosis (E) with respect to the patients with MCA stenosis (I). In F, box plot of the LI shows higher values of lateralization in the extra-cranial group.

Degree of stenoses confrontation

In order to understand the influence of the entity of the stenosis over the CVR, we made a statistical confrontation between the patients with significant stenoses and the subjects with slight stenoses, independently from its localization. For the carotid stenoses, we considered as significant the stenoses > 70 % according to the NASCET criteria.[43,44] For the middle cerebral artery stenoses, we considered them as significant if they exceeded the 50%.[45,46]

The group with not-significant stenoses consisted in 8 patients (mean age 70.88), with in the affected hemisphere a % Act Vox mean of 55.58% with St. Dv. 16.81, Z-max mean 10.60 with St. Dv. 2.18, Z-mean mean of 3.44 with St. Dv. 1.15 and LI mean of 0.04 with St. Dv. 0.03.

The group with severe stenoses consisted in 13 patients (mean age 58.31), with, in the affected hemisphere, a % Act Vox mean of 43.40% with St. Dv. 18.05, Z-max mean 8.87 with St. Dv. 1.70, Z-mean mean of 2.68 with St. Dv. 0.90 and LI mean of 0.20 with St. Dv. 0.12.

Despite the difference in the age mean, and the relative increase of the indexes values in the healthy hemisphere of the same patients, the mean values of the Activation Map indexes in the affected side of the patients with severe stenoses were averagely lower, with statistically significant difference of the Z-mean LI ($p < 0.05$) (fig. 7).

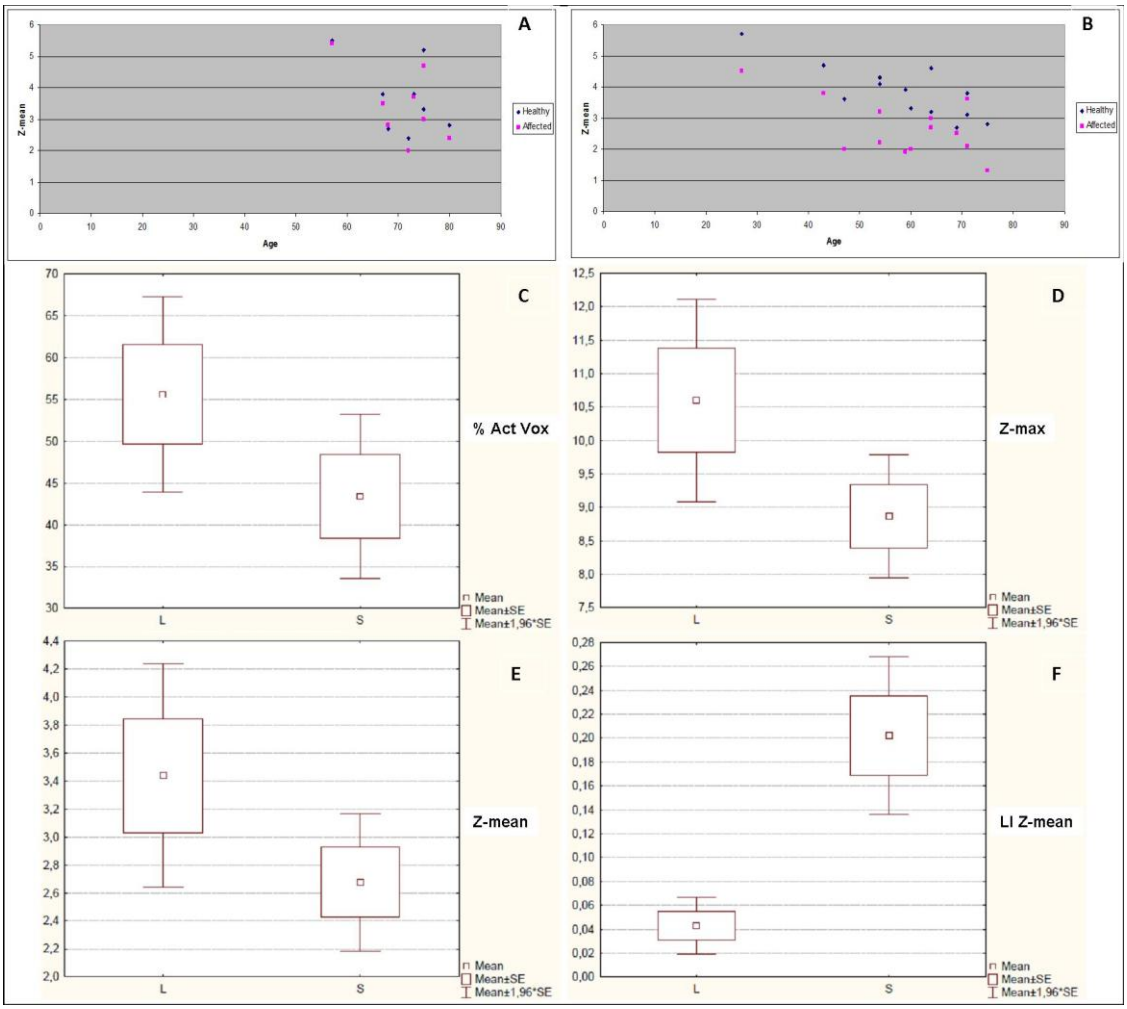

Figure 7. Confrontation between slight and severe stenoses. In A and B, scatter plots of the Z-mean shows higher dispersivity between healthy and affected hemisphere in the severe stenoses group. In C-E, box plots shows lower values of the Activation Map parameters in the patients with severe stenosis (S) with respect to the patients with light stenosis (L). In F, box plot of the LI shows higher values of lateralization in the severe stenoses group.

Relationship with the blood flow

With this analysis we tried to understand how the cerebral blood flow (CBF) and the CVR are related. The data of CBF obtained with ASL sequences in the affected hemispheres for all the patients have resulted for a mean 36.58 milliliters for minute (ml/min), median 33.65 ml/min, St. Dv. 13.28 ml/min with a confidence interval of 5.68 ml/min.

The correlation coefficient (*r*) was calculated among the CBF values and the indexes of the Activation Map of the affected hemisphere both using as reference the ROIs placed in the MCA territory and the ROIs in the PCA territory. We found a weak/moderate positive correlation, more pronounced for the Z-mean values (r = 0.56 using MCA ROI as reference and r = 0.62 using PCA ROI as reference) (fig. 8).

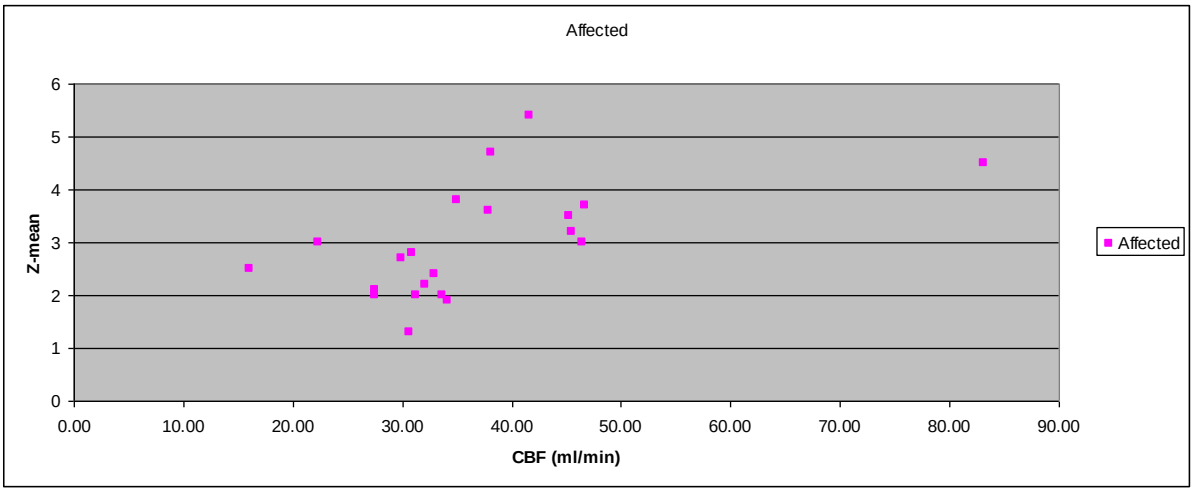

Figure 8. Correlation between CBF and Z-mean in the affected hemisphere considering as references for BOLD response ROIs in the MCA territory of the healthy hemispheres.

Confrontation with Doppler data: construction of ROC curves

In order to validate our method with respect to the TCD examination we elaborated Receiver Operating Characteristics (ROC) curves[47] from the Z-mean data obtained using as reference the ROI placed in the cortex of the temporal lobe of the healthy hemisphere. The number of patients which had performed a diagnostic TCD was 10. Consequently we included in the analysis 20 hemispheres, considering as true positive (TP) the hemisphere with CVR compromised at TCD. For this reason, the hemispheres of the two patients with bilateral CVR impairment were both considered TP while the hemispheres of the patients with unilateral CVR reduction were considered one TP and one True Negative (TN), according to the side of the CVR impairment.

Definitely, The TN group consisted of 14 hemispheres and the TP group of 6 hemispheres. The relative ROC curve had an Area under the curve of 0.8155, Cutpoint = 2.7, Sensivity = 66.67% and specificity = 85.71%, with diagnostic accuracy = 80% (fig. 9A)

In order to avoid the magnification of the results obtained considering in the analysis the hemisphere in which was placed the reference ROI, we elaborated another ROC curve considering only the contralateral hemispheres. In this analysis the TN group consisted of 6 hemispheres while the TP group of 6 hemispheres.

The relative ROC curve had an Area under the curve of 0.7500, Cutpoint = 2.5, Sensivity = 75.00% and specificity = 66.67%, with diagnostic accuracy = 70% (fig. 9B).

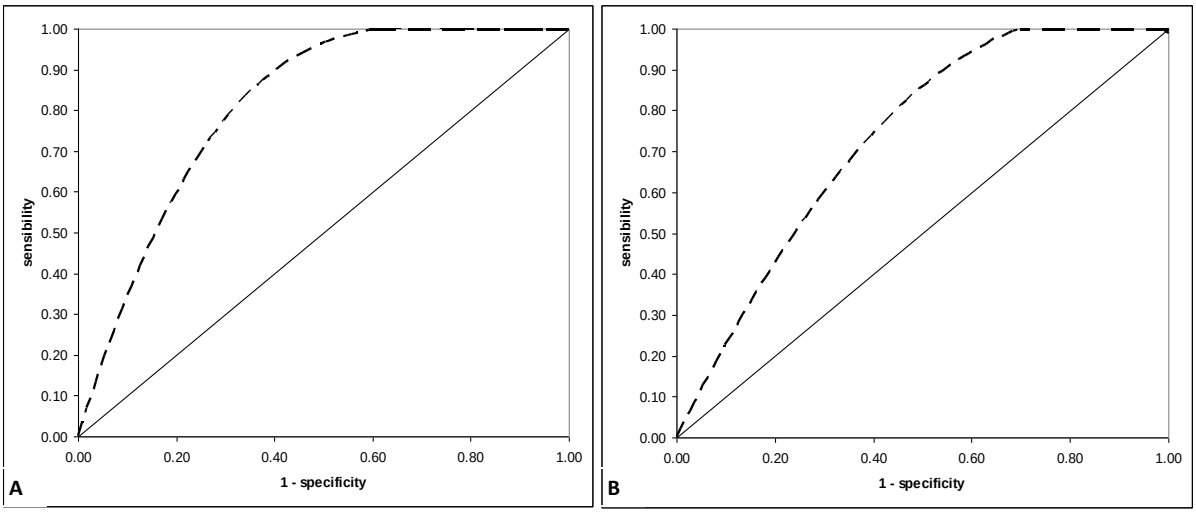

Figure 9. ROC curves generate from the confrontation of Z-mean and TCD data. In A, ROC curve with n = 20, with diagnostic accuracy = 80%. In B, ROC curve with n = 10, with diagnostic accuracy = 70%.

DISCUSSION

The assessment of Cerebral Vasoreactivity is crucial in order to identify, in a large population of patients with cerebropetal vessels stenosis, those most at risk to develop cerebrovascular accidents. Unfortunately the idea to screen this population with the most sensitive method, the ^{15}O-labeled PET, is far from reality, for the complexity of the methodic and possibility to perform the examination only in few centers. For this reason, TCD has become the only method to assess CVR in most of the cases, with the restrictions due to the only measurement of the flow velocity in the large vessels that constitutes a limited and indirect index of the CVR and to the possibility to do not perform a diagnostic examination because of the patient-dependence, the limited insonation window and signal quality.[12] Indeed, among the 12 patients of our study who performed TCD, in two cases (16.7%) the

examination resulted not diagnostic because of the aliasing artifacts. Moreover, recent studies challenge the assessment of CVR impairment by using the TCD as predictor of risk of cerebrovascular accidents.[35,48]

The possibilities offered by Magnetic Resonance Imaging as diagnostic tool for the assessment of CVR are manifold, in particular f-MRI, perfusional imaging and Susceptibility Weighted Imaging (SWI) are potentially capable of evaluate CVR or the Oxygen Extraction Fraction.[49,50] In our study, we used the f-MRI because of its higher temporal resolution that allows the possibility of build a protocol totally not-invasive. The breath-hold exercise, with a relatively short duration (7 minutes) and little periods of apnea (15 seconds) was well tolerated and completed by all the patients.

The multiple possibilities of analysis of the f-MRI acquisitions provided a huge mole of data that open possibilities not only in the assessment of the CVR but also in understanding the pathophysiology of the microcirculation of the patients with intra-cranial and extra-cranial stenosis. We focused on the data obtained in the "healthy" hemisphere in order to understand the differences of CVR along the brain and the influence of age and the principal risk factors, then we examined the differences between healthy and affected hemisphere trying to relate the alterations of the BOLD response to the location and the degree of the stenosis and the data provided by the perfusional sequences. Finally, we tried to use the limited data of the TCD, considered "the reference method", to create ROC curves, waiting for more data in order to improve the diagnostic accuracy of the method.

Healthy hemisphere. Influence of age and comorbidities.

As could be expected, we found a negative correlation, although moderate, between the age and the magnitude of the response of the stimulus, suggestive of a progressive impairment of the CVR in the oldest people, regardless of the presence or the degree of a stenosis of the main cerebropetal vessels and probably due to pathology of the microcirculation.[51] However, the analysis of the BOLD indexes obtained in the small ROIs placed by the radiologist in the cortex of the temporal lobe in which he observed the best response seems to offer conflicting data. In particular, the Maximum Peak had a moderate positive correlation with the age. This observation, although with low statistical robustness, could reflect the in the oldest the CVR has an irregular pattern along the brain, with areas more responsive to the vasodilator stimulus and areas less reactive, but with a globally reduction of the CVR.

Considering the comorbidities, we did not find statistically significant relationship with the CVR, although mean lower values of the response has been found in hypertension,

dyslipidemia and smokers (the number of diabetic patients was extremely low, only 3). A larger number of patients or a less heterogeneous group for degree of vessel pathology could allow more confident conclusions.

Healthy vs affected hemispheres analyses

The differences of the response between the two hemispheres, statistically validated with *t-test*, are a good index of the sensibility of the f-MRI the evaluation of CVR. The differences in percentage of activated voxels and magnitude could be easily quantified with the Laterality Index. However, LI does not provide absolute values and could be a confounding index in patients with bilateral stenoses or in patients with asymmetric response but CVR still preserved in the affected hemisphere (fig 10). For this reason, the identification of an independent index able to quantify the CVR independently from the other hemisphere is crucial. Among the Activation Map parameters, the Z-mean seems to be the most reliable, considering the dependence of the % Act Vox from the threshold and the higher dependence of the Z-max from the reference ROI if placed in the anterior circulation territory.

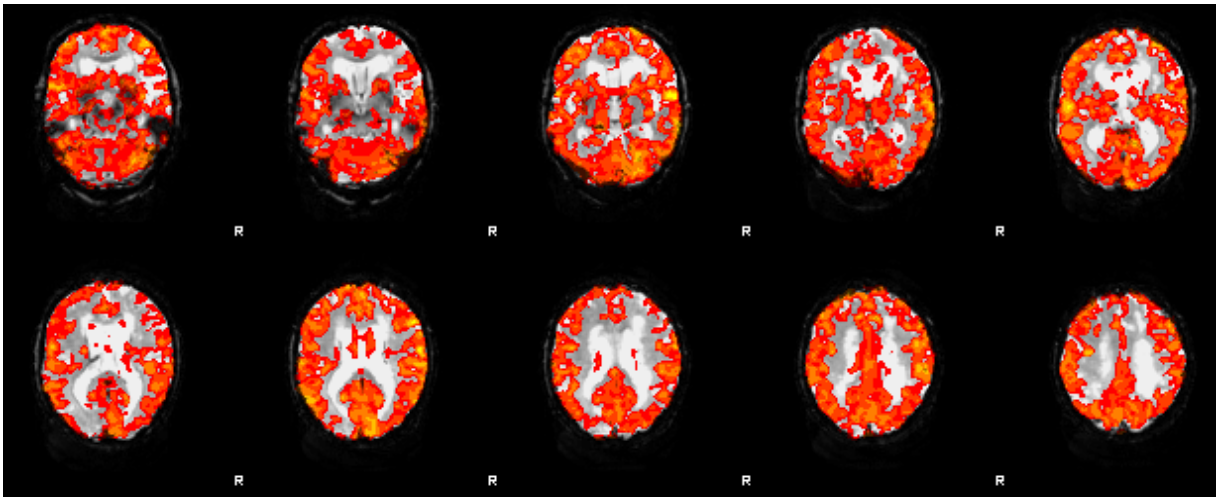

Figure 10. Activation Map of the patient 2 (male, 75 y.o.) with bilateral and symmetric percentage of Activated Voxel could suggest a normal CVR. Instead the patient, affected by bilateral MCA stenosis, presented bilateral CVR impairment, demonstrated at TCD.

Concerning the location of the stenoses, we found higher difference between healthy and affected side in the patients with extra-cranial stenosis, although not statistically significant. This aspect could be explained by the fact that the vascular territory of the carotid artery is larger than the MCA vascular territory. However, this supposition needs more data to be validated, considering that the difference of the two groups could be explained by the fact that in the MCA group 5 of 10 patients were affected by severe stenosis while in the ICA group the patients with significant stenosis were 8 of 10.

About the degree of the stenosis, the influence over the CVR seems to be more important, with statistically significant higher values of the Z-mean LI in the group with severe stenoses of the intra or extra-cranial vessels. However, while we did not find particular impairment of the CVR in the subjects with mild stenosis, the pattern of response in the group with significant stenosis is more heterogeneous, with patients affected by severe vessel narrowing but with perfect CVR response (fig. 11 A-B). This observation seems to prove that CVR values provided by f-MRI are not a mere reflection of the entity of the stenosis.

Similarly, the perfusional data suggest the same conclusion. The correlation coefficient calculation between the values of the basal cerebral blood flow and the Z-mean suggested a weak/moderate positive correlation. Vessels stenoses bring to reduction of the basal CBF as well as the CVR, but the relationship between the three variables is not always predictable (fig. 11 C-D).

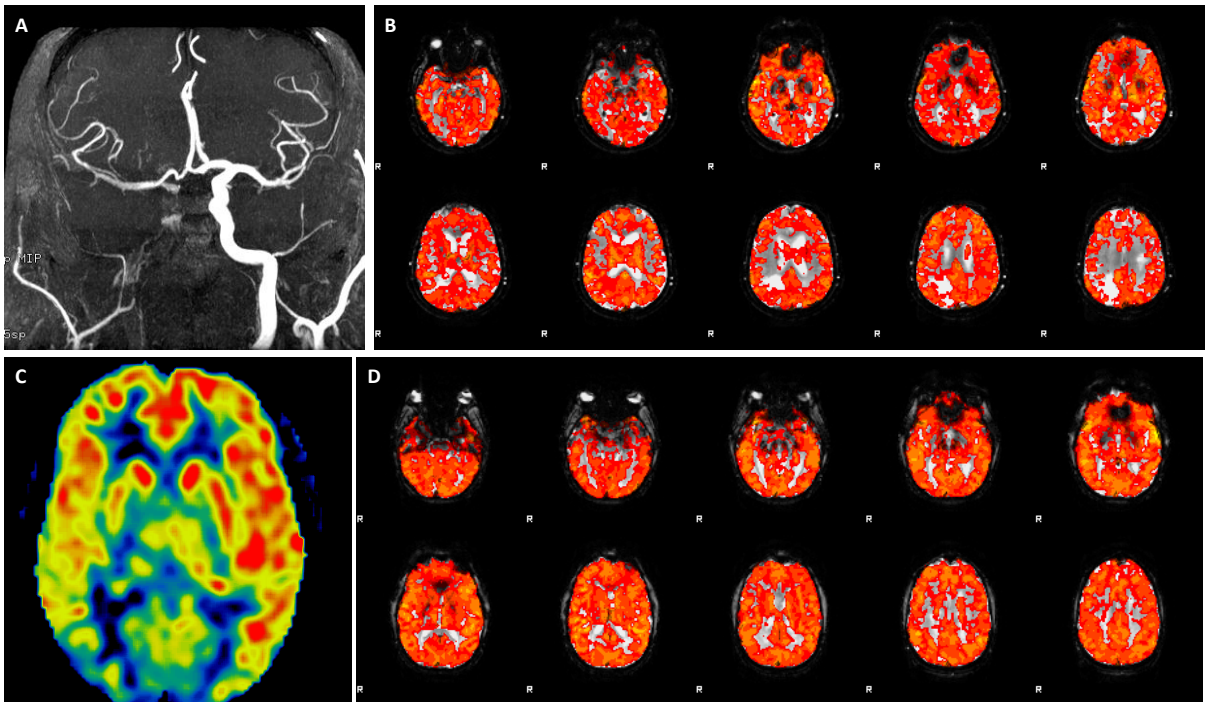

Figure 11. In A, 3D-INHANCE MR-Angiography of pt 20 (male, 70 y.o.) show right internal carotid occlusion. In B, Activation Map of the same patient do not show CVR impairment in the ipsilateral hemisphere. In C, ASL perfusion images of pt 1 (male, 57 y.o.), affected by right MCA stenosis, demonstrate reduction of basal CBF in the ipsilateral hemisphere. In D, Activation Map of the same patient show bilateral activation with no CVR impairment, as demonstrated also with TCD.

Comparison with Doppler data

Although TCD is longer to be the gold standard, it is the most used method to assess the CVR. For this reason we considered it as reference method and we compared the results of the TCD performed in 10 patients of our casuistry with the results of the f-MRI obtained from the same patients in order to calculate the accuracy coefficient of our method.

Unfortunately the scarce number of patient with a diagnostic TCD did not allow to elaborate ROC curve with high value of specificity and sensibility. The best diagnostic accuracy (80%) was reached by comparing TCD and the Z-mean. However, a larger number of TCD is necessary to draw more robust conclusions.

Two TCD resulted not diagnostic because of aliasing artifacts. F-MRI data suggested in one of these patient a severe impairment of the CVR, an example of the potential superiority of this method with respect to the ultrasound (fig. 12).

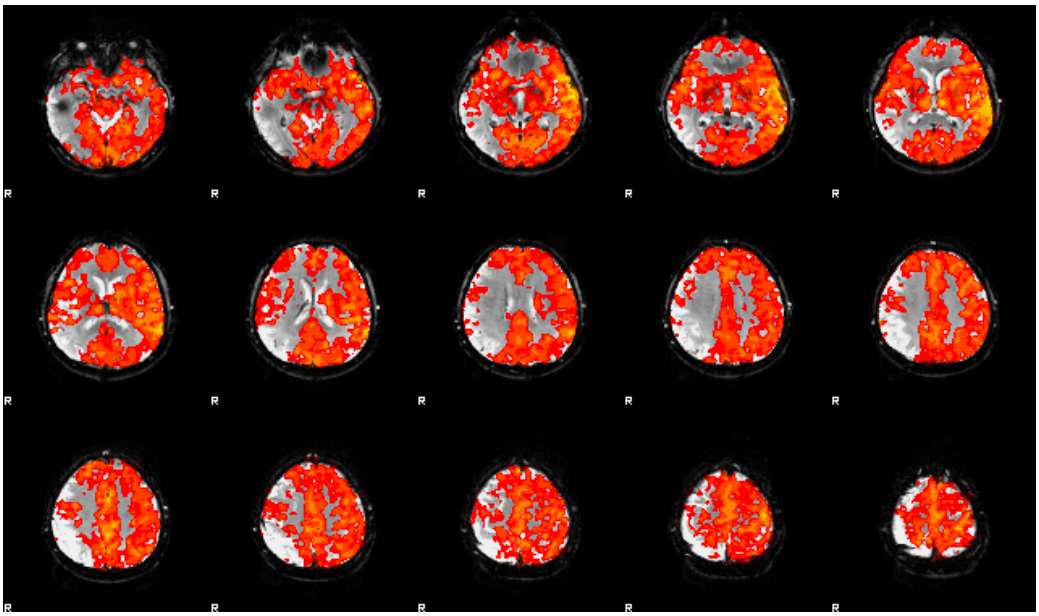

Figure 12. Activation Map of the pt 11 (male, 64 y.o.), affected by right MCA severe stenosis (see fig. 3A), who performed TCD that resulted not diagnostic because of aliasing artifacts. In this case f-MRI demonstrated CVR impairment of the right hemisphere, ipsilateral to the stenosis.

Limits of the study

One of the principal limitation of our study is the heterogeneity of our population, considering degree and localization of the stenoses, age and comorbidities. The high number of variables that could influence the CVR should be minimized or at least uniformed in order to have a more exact perception of the BOLD response values. For the same reason, the assumption to consider as "healthy" the hemisphere contralateral to the side affected by the ICA or MCA stenosis, as we made in our study, is a stretch, due to the lack of reference values on a healthy population. A study on a healthy population using the same protocol is desirable and theoretically should have been performed before, in order to elaborate a reference Activation Map with respect to which the data of the affected should have been compared.

Finally, the number of TCD is to date too low to make significant comparison with f-MRI. However this limit could be easily overcome by recruiting for the Doppler the rest of our population, as planned in the design of the study.

CONCLUSIONS

f-MRI with breath-hold paradigm is a promising alternative tool in the assessment of cerebral vasoreactivity. Its main advantages are the non-invasiveness, the operator-indipendence and the possibility to perform in the same examination also morphologic and angiographic sequences for a complete evaluation of brain parenchima and circulation. The analyses of the f-MRI data underlined the sensibility in differentiate healthy and affected hemispheres for the BOLD response and Activation Map indexes and point out new information in the evaluation of the microcirculation. The measurement of BOLD response could also be helpful in the assessment of cerebral vasoreactivity in the subjects in which the trans-cranial Doppler examination is doubt, not diagnostic or not practicable.

REFERENCES

1. Krainik A, Villien M, Troprès I, et al. Functional imaging of cerebral perfusion. *Diagn Interv Imaging*. 2013; 94:1259-1278.

2. Girouard H, Iadecola C. Neurovascular coupling in the normal brain and in hypertension, stroke, and Alzheimer disease. *J Appl Physiol*. 2006; 100:328-335.

3. Devonshire IM, Papadakis NG, Port M, et al. Neurovascular coupling is brain region-dependent. *Neuroimage*. 2012; 59:1997-2006.

4. Touzani O, Mackenzie ET. Physiology and pathology of cerebral and spinal circulation. *Neurol Clin Neurosci*. 540-549.

5. Ho SSY, Lam WWM, Ng SCP, et al. Cerebral vasoreactivity: A comparison of color velocity imaging quantification and stable xenon-enhanced CT. *Am J Roentgenol*. 2005; 184:948-952.

6. Bright MG, Murphy K. Reliable quantification of BOLD fMRI cerebrovascular reactivity despite poor breath-hold performance. *Neuroimage*. 2013; 83:559-568.

7. Corfield DR, Murphy K, Josephs O, et al. Does hypercapnia-induced cerebral vasodilation modulate the hemodynamic response to neural activation? *Neuroimage*. 2001; 13:1207-1211.

8. Posse S, Olthoff U, Weckesser M, et al. Regional dynamic signal changes during controlled hyperventilation assessed with blood oxygen level-dependent functional MR imaging. *Am J Neuroradiol*. 1997; 18:1763-1770.

9. Inoue Y, Tanaka Y, Hata H, Hara T. Arterial spin-labeling evaluation of cerebrovascular reactivity to acetazolamide in healthy subjects. *Am J Neuroradiol*. 2014; 35:1111-1116.

10. Webster MW, Makaroun MS, Steed DL, et al. Compromised cerebral blood flow reactivity is a predictor of stroke in patients with symptomatic carotid artery occlusive disease. *J Vasc Surg Off Publ Soc Vasc Surg*. 1995; 21:338-345.

11. Yonas H, Smith H a, Durham SR, et al. Increased stroke risk predicted by compromised cerebral blood flow reactivity. *J Neurosurg*. 1993; 79:483-489.

12. Novak V, Hajjar I. The relationship between blood pressure and cognitive function. *Nat Rev Cardiol*. 2010; 7:686-698.

13. Kuwabara Y, Ichiya Y, Sasaki M, et al. PET evaluation of cerebral hemodynamics in occlusive cerebrovascular disease pre- and postsurgery. *J Nucl Med*. 1998;39:760-765.

14. Chang TY, Liu HL, Lee TH, et al. Change in cerebral perfusion after carotid angioplasty with stenting is related to cerebral vasoreactivity: a study using dynamic susceptibility-weighted contrast-enhanced MR imaging and functional MR imaging with a breath-holding paradigm. *AJNR Am J Neuroradiol*. 2009; 30:1330-1336.

15. Marshall RS, Hacein-Bey L, Young WL, et al. Functional reorganization induced by endovascular embolization of a cerebral AVM. *Hum Brain Mapp*. 1996; 4:168-173.

16. Klinge PM, Berding G, Brinker T, et al. A positron emission tomography study of cerebrovascular reserve before and after shunt surgery in patients with idiopathic chronic hydrocephalus. *J Neurosurg*. 1999; 91:605-609.

17. Nagata K, Buchan RJ, Yokoyama E, et al. Misery perfusion with preserved vascular reactivity in Alzheimer's disease. *Ann N Y Acad Sci*. 1997; 826:272-281.

18. Pávics L, Grünwald F, Reichmann K, et al. Regional cerebral blood flow single-photon emission tomography with ^{99}mTc-HMPAO and the acetazolamide test in the evaluation of vascular and Alzheimer's dementia. *Eur J Nucl Med*. 1999; 26:239-245.

19. Powers WJ, Raichle ME. Positron emission tomography and its application to the study of cerebrovascular disease in man. *Stroke*. 2015; 16:361-376.

20. Gupta A, Marshall S. Moving Beyond Luminal Stenosis : Imaging Strategies for Stroke Prevention in Asymptomatic Carotid Stenosis. *Cerebrovasc Dis* 2015:253-261.

21. Herzig R, Hlustík P, Skoloudík D, et al. Assessment of the cerebral vasomotor reactivity in internal carotid artery occlusion using a transcranial Doppler sonography and functional MRI. *J Neuroimaging*. 2008; 18:38-45.

22. Markus HS, Harrison MJ. Estimation of cerebrovascular reactivity using transcranial Doppler, including the use of breath-holding as the vasodilatory stimulus. *Stroke*. 1992; 23:668-673.

23. Purkayastha S, Sorond F. Transcranial Doppler Ultrasound: Technique and Application. *Semin Neurol.* 2014; 32:411-420.

24. Hajjar I, Zhao P, Alsop D, Novak V. Hypertension and cerebral vasoreactivity: A continuous arterial spin labeling magnetic resonance imaging study. *Hypertension*. 2010; 56:859-864.

25. Ferré JC, Bannier E, Raoult H, et al. Arterial spin labeling (ASL) perfusion: techniques and clinical use. *Diagn Interv Imaging*. 2013; 94:1211-1223.

26. Dahl A, Russel D, Rootwelt K, et al. Cerebral vasoreactivity assessed with transcranial Doppler and regional cerebral blood flow measurements. Dose, serum concentration, and time course of the response to acetazolamide. *Stroke*. 1995; 26:2302-6.

27. Rostrup E, Law I, Blinkenberg M, et al. Regional differences in the CBF and BOLD responses to hypercapnia: a combined PET and fMRI study. *Neuroimage*. 2000; 11:87-97.

28. Haller S, Bonati LH, Rick J, et al. Reduced cerebrovascular reserve at CO^2 BOLD MR imaging is associated with increased risk of periinterventional ischemic lesions during carotid endarterectomy or stent placement: preliminary results. *Radiology*. 2008; 249:251-258.

29. Heyn C, Poublanc J, Crawley a., et al. Quantification of cerebrovascular reactivity by blood oxygen level - Dependent MR imaging and correlation with conventional angiography in patients with moyamoya disease. *Am J Neuroradiol*. 2010;31(5):862-867.

30. Chang TY, Kuan WC, Huang KL, et al. Heterogeneous Cerebral Vasoreactivity Dynamics in Patients with Carotid Stenosis. *PLoS One*. 2013; 8:1-10.

31. Mandell DM, Han JS, Poublanc J, et al. Mapping cerebrovascular reactivity using blood oxygen level-dependent MRI in patients with arterial steno-occlusive disease: Comparison with arterial spin labeling MRI. *Stroke*. 2008; 39:2021-2028.

32. Smith SM, Zhang Y, Jenkinson M, et al. Accurate, robust, and automated longitudinal and cross-sectional brain change analysis. *Neuroimage*. 2002; 17:479-489.

33. Jenkinson M, Smith S. A global optimisation method for robust affine registration of brain images. *Med Image Anal*. 2001; 5:143-156.

34. Jenkinson M, Bannister P, Brady M, Smith S. Improved optimization for the robust and accurate linear registration and motion correction of brain images. *Neuroimage*. 2002; 17:825-841.

35. Jolink WMT, Heinen R, Persoon S, et al. Transcranial Doppler Ultrasonography CO^2 Reactivity Does Not Predict Recurrent Ischaemic Stroke in Patients with Symptomatic Carotid Artery Occlusion. *Cerebrovasc Dis*. 2014; 37:30-37.

36. Reinhard M, Briel M, Altamura C, et al. Cerebrovascular reactivity predicts stroke in high-grade carotid artery disease. *Neurology*. 2014; 83:1424-31.

37. Marks MP, Pelc NJ, Ross MR, et al. Determination of cerebral blood flow with a phase-contrast cine MR imaging technique: evaluation of normal subjects and patients with arteriovenous malformations. *Radiology*. 1992; 182:467-476.

38. Bash S, Villablanca JP, Jahan R, et al. Intracranial vascular stenosis and occlusive disease: evaluation with CT angiography, MR angiography, and digital subtraction angiography. *Am J Neuroradiol*. 2005; 26:1012-1021.

39. Cyprian I, Oyeka A, Ebuh GU. Modified Wilcoxon Signed-Rank Test. *Open J Stat*. 2012; 2012:172-176.

40. Fay MP, Proschan MA. Wilcoxon-Mann-Whitney or t-test? On assumptions for hypothesis tests and multiple interpretations of decision rules. *Stat Surv*. 2010; 4:1-39.

41. Jansen A, Menke R, Sommer J, et al. The assessment of hemispheric lateralization in functional MRI-Robustness and reproducibility. *Neuroimage*. 2006; 33:204-217.

42. Jones SE, Mahmoud SY, Phillips MD. A practical clinical method to quantify language lateralization in fMRI using whole-brain analysis. *Neuroimage*. 2011; 54:2937-2949.

43. Nederkoorn PJ, van der Graaf Y, Eikelboom BC, et al. Time-of-Flight MR Angiography of Carotid Artery Stenosis: Does a Flow Void Represent Severe Stenosis? *Am J Neuroradiol*. 2002; 23:1779-1784.

44. Ota H, Takase K, Rikimaru H, et al. Quantitative vascular measurements in arterial occlusive disease. *Radiographics*. 2005; 25:1141-1158.

45. Baumgartner RW, Mattle HP, Schroth G. Assessment of >=50% and <50% Intracranial Stenoses by Transcranial Color-Coded Duplex Sonography. *Stroke*. 1999; 30:87-92.

46. Huang HW, Guo MH, Lin RJ, et al. Prevalence and risk factors of middle cerebral artery stenosis in asymptomatic residents in Rongqi County, Guangdong. *Cerebrovasc Dis*. 2007; 24:111-115.

47. Zweig MH, Campbell G. Receiver-operating characteristic (ROC) plots: a fundamental evaluation tool in clinical medicine. *Clin Chem*. 1993; 39:561-577.

48. Portegies MLP, De Bruijn RFAG, Hofman A, et al. Cerebral vasomotor reactivity and risk of mortality : the rotterdam study. *Stroke*. 2014; 45:42-47.

49. Zaitsu Y, Kudo K, Terae S, et al. Mapping of Cerebral Oxygen Extraction Fraction Changes with Susceptibility-weighted Phase Imaging. *Radiology*. 2011; 261:930-936.

50. Chang K, Barnes S, Haacke EM, et al. Imaging the effects of oxygen saturation changes in voluntary apnea and hyperventilation on susceptibility-weighted imaging. *Am J Neuroradiol*. 2014; 35:1091-1095.

51. Farkas E, Luiten PG. Cerebral microvascular pathology in aging and Alzheimer's disease. *Prog Neurobiol*. 2001; 64:575-611.